A STUDY ON FEMU: INFLUENCE OF SELECTION OF EXPERIMENTS ON RESULTS FOR ABS-M30 MATERIAL

JAROSLAV ROJICEK, ZBYNEK PASKA, MARTIN FUSEK, FRANTISEK FOJTIK, DAGMAR LICKOVA

Department of Applied Mechanics, Faculty of Mechanical Engineering, Ostrava-Poruba, Czech Republic

DOI: 10.17973/MMSJ.2021_12_2021113

Jaroslav.rojicek@vsb.cz

This paper examines the effect of experiments used to identify material parameters of a more complex material model (12 material parameters). The set of experiments includes tensile tests and indentation tests with different loading conditions at 4 different temperatures (a total of 14 experiments) for the ABS-M30 material. The behaviour of the material was simulated using Anand's material model, and the Finite Element Model Updating approach was used to identify the material parameters. The parameters are solved for 3 variants: identification from indentation tests, identification from tensile tests, identification from all experiments. For the first two variants, the remaining experiments are used to verify. Finally, all results are compared.

KEYWORDS

FEMU, tension tests, indentation tests, Anand material model, ABS-M30, influence of experiments,

1 INTRODUCTION

The historical approach to material parameters identification is hardly attached to the material model. For a given material model, there were usually defined experiments, which are used in the identification process. Thus, determination of material parameters was part of the design of the material model [Brown 1989]. This procedure was based on the analytical solution of the experiments, often tensile tests at different temperatures, speeds, etc.

An inverse identification is a reversed approach based on an iterative process. In this method the material parameters input into a Finite Element (FE) model of an experiment are iteratively updated. The objective is a minimisation of differences between corresponding experimental data and data obtained from their simulations (FEM). The FEM Updating (FEMU) methods use for minimalisation two basic aproaches, gradient methods and evolutionary or genetic algorithms (EA or GA) [Anrade 2007], [Moslemi 2020]. The advantage of FEMU is easy simulation of even more complex stress states (eg indentation [Inoue 2015]), use of more experiments, noproportionate loading [Rojicek 2021], etc.

Determination of material parameters for Anand's model is described for example in: [Brown 1989] by compression tests, [Grama 2015] by a Virtual Fields Method and shear tests, [Rodgers 2005] by tensile tests, etc. Indentation is also used to determine material parameters [Inoue 2015]. Different experiments can also be used to verify the results, for example Four-point bending test [Yap 2019]. FEMU allows the use of groups of experiments to determine material parameters, see [Neggers 2019] or [Rojicek 2021].

FEMU approach is used for identification of material parameters from one or more experiments for a lot of different material models [He 2018], [Moslemi 2020], [Touzeau 2016], etc. These experiments can be divided into three different sets :

1. The experiments are determined by the material model [Brown 1989].
2. The experiments are not determined by the material model, for example: use of an indentation test [Inoue 2015], a punch stretch test [Li 2013], etc.
3. The experiments are determined by available data and may include the experiments referred to in points 1 and 2 [Rojicek 2021]. Some experiments may be redundant for the selected material model, others important for the material model may be missing.

The first and second points concern the solution of one selected material model. The third point concerns the solution of the selected material, which, depending on its application, can be described by different material models (linear elastic, elastic-plastic, fracture, fatigue, creep, etc.).

The main goal of the article is to test the influence of the selection of experiments on the result of the identification and whether the results obtained from the identification are comparable for different experiments. Two types of experiments are used for identification - tensile tests and indentation tests. The tensile test is one of the most commonly used and indentation tests are often used in combination with FEMU.

2 EXPERIMENTS

The experiments were published at first in [Fusek 2021], therefore they are described only briefly. Tensile tests graded tensile tests and indentation tests were performed. The experiments were performed on a Testometric M500-50CT (LABOR machine, s.r.o., Otice, Czech Republic). The sample shown in Figure 1 was used for all experiments, the indentation test was performed in the area shown by the dashed rectangle.

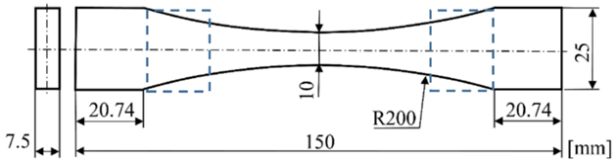

Figure 1. Specimen shape for simple and graded tensile tests.

2.1 *Tensile Tests*

All tensile tests were deformation-controlled and they were performed at four different temperatures (23 °C, 44 °C, 60 °C, and 80 °C) and at three different rates of deformation (0.017 mm/s, 0.167 mm/s, and 1.667 mm/s) until specimen failure. The data are shown in Figure 2. – Figure 4.

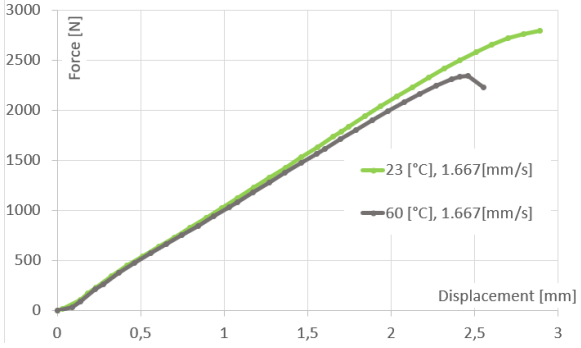

Figure 2. Tensile tests at 23 °C and 60 °C at a constant rate of deformation of 1.667 mm/s.

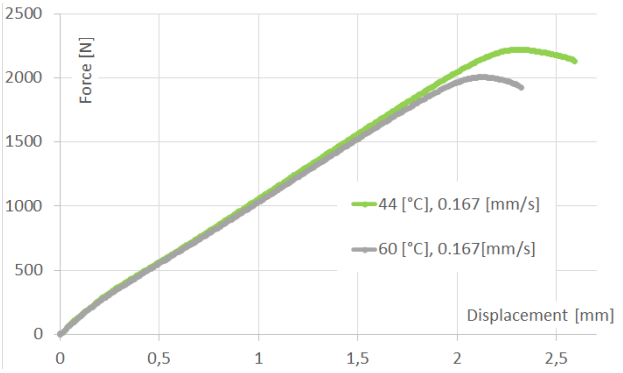

Figure 3. Tensile tests at 44 °C and 60 °C at a constant rate of deformation of 0.167 mm/s.

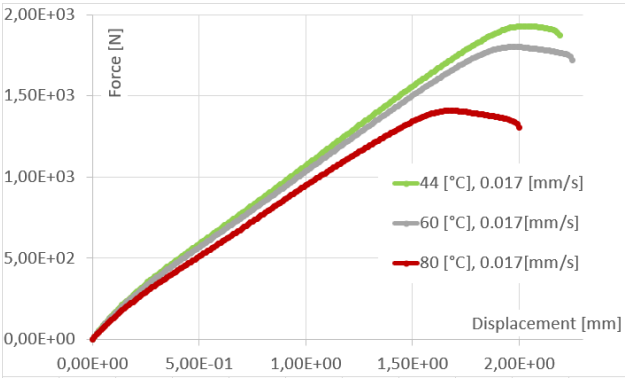

Figure 4. Tensile tests at temperatures of 44 °C, 60 ◦C, and 80 °C, with constant rates of deformation at 0.017 mm/s.

2.2 *Graded Tensile Tests*

Graded tensile tests were carried out at three different temperatures (44 °C, 60 °C, and 80 °C), with the same deformation step size of 0.25 mm. The specimen was elongated by 0.25 mm at each step, at a deformation rate of 0.017 mm/s. The time delay at the given strain value was always 60 s. This was done until the specimen failed. The data are shown in Figure 5.

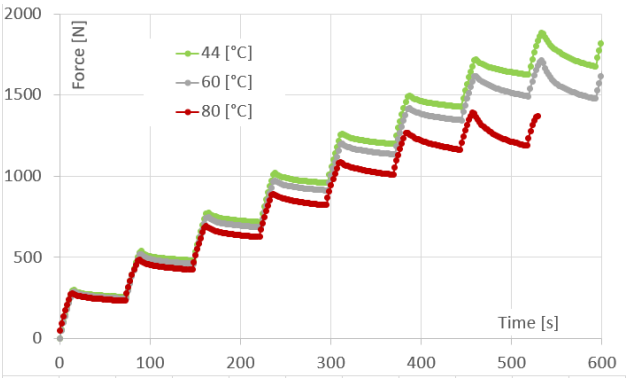

Figure 5. Graduated tensile tests under three different temperatures of 44 °C, 60 °C, and 80 °C.

2.3 *Indentation Tests*

Indentation tests were carried out at 23 °C, 44 °C, 60 °C and 80 °C on the samples depicted in Figure 2. The indenter was a steel sphere with a diameter of 5 mm. The indentation test consisted of three phases. First, the indenter was pressed into the material at a speed of 0.017 mm/s to a depth of 0.5 mm, then the time delay of 300 s followed, and finally the indenter returned to the starting position (relief) at the same speed. The data are shown in Figure 6.

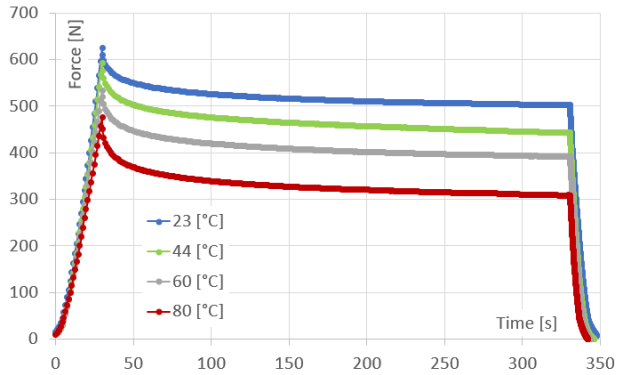

Figure 6. Indentation tests with time delay at temperatures of 23 °C, 44 °C, 60 °C, and 80 °C, with a constant indenter rate of 0.017 mm/s.

3 MATERIAL MODEL

Anand viscoplastic model was originally developed for material forming applications **[Anand 1985]**. It is also applicable to general viscosity problems that include the influence of strain rate and the influence of temperature. Materials at elevated temperatures are highly dependent on the influence of temperature magnitude and history, strain rate and strain hardening. The material model is given by 11 material parameters: Poisson ratio (μ), Young's modulus (E), Initial value of deformation resistance (s_0), Activation energy/Universal gas constant (Q/R), Pre-exponential factor (A), Stress multiplier (x_i), Strain rate sensitivity of stress (m), Hardening/softening constant (h_0), Coefficient for deformation resistance saturation value ($\hat{S}$), Strain rate sensitivity of saturation (deformation resistance) value (n) and Strain rate sensitivity of hardening or softening (a). Regarding the temperatures used, the total number of parameters is extended to $N_p = 12$ as follows:

$$X = \left\{E_{20}, E_{80}, \mu, s_0, \frac{Q}{R}, A, x_i, m, h_0, \hat{S}, n, a\right\}. \quad (1)$$

Where X is a vector of material parameters, and E_{20}, E_{80} are Young's modulus for temperatures 20 °C and 80 °C, respectively. The model of Anand is a complex material model that has introduced an internal variable S (deformation resistance), a variable that represents the resistance against the plastic behaviour of the material. The rate of plastic deformation is described by the following relationship:

$$\dot{\boldsymbol{\varepsilon}}_{pl} = \dot{\varepsilon}^{a}{}_{pl}\left(\frac{3}{2}\frac{\mathbf{S}}{q}\right), \quad (2)$$

where $\dot{\boldsymbol{\varepsilon}}_{pl}$ is the tensor of the inelastic strain rate and $\dot{\varepsilon}^{a}{}_{pl}$ is the rate of accumulated equivalent plastic strain. $\dot{\varepsilon}^{a}{}_{pl}$ is given by the equation:

$$\dot{\varepsilon}^{a}{}_{pl} = \left(\frac{2}{3}\,\dot{\boldsymbol{\varepsilon}}_{pl} : \dot{\boldsymbol{\varepsilon}}_{pl}\right)^{\frac{1}{2}}, \quad (3)$$

where the operator ":" stands for inner product of tensors. $\mathbf{S}$ is the deviator of Cauchy stress tensor, which can be expressed by the following relation:

$$\mathbf{S} = \boldsymbol{\sigma} - p\mathbf{I}, \quad (4)$$

where $\boldsymbol{\sigma}$ is the Cauchy stress tensor, p is defined as one third of the trace of the tensor matrix $\boldsymbol{\sigma}$, see the following relation:

$$p = \frac{1}{3}\mathrm{tr}(\boldsymbol{\sigma}). \quad (5)$$

$\mathbf{I}$ represents a second order unit tensor. The quantity q is the equivalent stress according to the following relation:

$$q = \left(\frac{3}{2}\mathbf{S} : \mathbf{S}\right)^{\frac{1}{2}}. \quad (6)$$

The rate of accumulated plastic deformation depends on q and on the internal state variables s. This dependence can be expressed by the following relation:

$$\dot{\varepsilon}^{a}{}_{pl} = A e^{\left(-\frac{Q}{R\theta}\right)} \left\{\sinh \xi \frac{q}{s}\right\}^{\frac{1}{m}}. \quad (7)$$

In the expression (6) A, ξ and m are the model constants, Q the activation energy, R the universal gas constant, θ the absolute temperature and s the internal state variable. The development of the internal state parameter s is described as follows:

$$\dot{s} = \oplus h_o \left|1 - \frac{s}{s^*}\right|^a \dot{\varepsilon}^{a}{}_{pl}, \quad (8)$$

where a and h_o are constants, s^* represents the saturated value of the internal parameter. The $\oplus$ operator is defined to return $+1$ if $s \leq s^*$, otherwise return -1. The saturation values of s^* depend on the rate of equivalent plastic deformation $\dot{\varepsilon}^{a}{}_{pl}$ and can be expressed as follows:

$$s^* = \hat{s}\left\{\frac{\dot{\varepsilon}^{a}{}_{pl}}{A} e^{\left(\frac{Q}{R\theta}\right)}\right\}^n, \quad (9)$$

where $\hat{s}$ and n represent constants.

The initial parameters for identification are taken from in [Fusek 2021] and shown in Table 1. In the paper, the Young's modulus was determined only for two temperatures $\mathbf{E_{20}}$, $\mathbf{E_{80}}$, with the same initial value 1750 MPa.

Parameter p_k	E_{20} [MPa]	E_{80} [MPa]	μ [–]	s_0 [MPa]
k	1	2	3	4
Value	1780	1780	0.33	19.54
Parameter p_k	Q/R [K]	A [1/s]	x_i	m [–]
k	5	6	7	8
Value	8350	3134	5.18	0.2466
Parameter p_k	h_0 [MPa]	$\hat{S}$ [MPa]	n [–]	a [–]
k	9	10	11	12
Value	183245	31.0	0.0098	1.524

Table 1. Marking and initial values of parameter.

In general, we will call the material parameters as follows:

$$X = \left\{p_k, k = \{1,2, \dots, N_p\}\right\}, \quad (10)$$

where, for the material model are $p_1 = \mathbf{E_{20}}$, $p_2 = \mathbf{E_{80}}$, etc., as is shown in Table 1. This notation is used in Chapter 4 to describe the theory.

4 MATERIAL PAREMETERS IDENTIFICATION

Determination of material parameters can be described as follows:

FIND X,
MINIMIZE f(X), (11)
SUBJECT TO $p_k \in \langle p_{k,min}, p_{k,max}\rangle, \forall\, p_k \in X,$

where $p_{k,min}, p_{k,max}$ are constraints of parameters and f(X) is an objective function.

4.1 *Objective function*

The objective function for all experiments f(X) was calculated as:

$$f(X) = \sqrt{\frac{\sum_{i=1}^{N} f_i(X)^2}{N}}, \quad (12)$$

where N is several experiments, $f_i(X)$ is a partial objective function for i-th experiment. The objective function will be simply denoted as $f = f(X)$. The partial objective function describes a difference between experimental data and data from simulation model and it is calculated as follows:

$$f_i(X) = \frac{\sum_{j=1}^{N_i} |F_{i,j}^{EXP} - F_{i,j}^{FEM}(X)|}{\sum_{j=1}^{N_i} |F_{i,j}^{EXP}|}, i = \{1,2,3, \dots, N\} \quad (13)$$

N_i is a number of measurement points for i-th experiment, $F_{i,j}^{EXP}$ is an experimental force, $F_{i,j}^{FEM}(X)$ is a force obtained from the simulation.

4.2 *Sensitivity analysis*

Sensitivity analysis is used to determine the influence of individual parameters on the value of the objective function. For the set of experiments, we can also determine the influence of individual parameters on the value of the partial objective function, or whether the set of experiments is suitable for identification of parameters for the selected material model.

At first, we define a change of the material parameter Δp_k from p_k using a sensitivity coefficient k_{Sen} as follows:

$$\Delta p_k = k_{Sen}\, p_k, \forall\, p_k \in X, \quad (14)$$

The value of the sensitivity coefficient is the same for all parameters. To simplify, the following notation will be used:

$$\begin{aligned} &p_{+\Delta k} = p_k(1 + k_{Sen}), p_{-\Delta k} = p_k(1 - k_{Sen}), \\ &f_{+\Delta k} = f(\{p_1, \dots, p_{+\Delta k}, \dots, p_{Np}\}), \\ &f_{-\Delta k} = f(\{p_1, \dots, p_{-\Delta k}, \dots, p_{Np}\}). \end{aligned} \quad (15)$$

The value of senitivity is zero if the parameter (or the experiment etc.) has no effect on the value of the objective function. Conversely, the higher the sensitivity value, the greater the influence of the investigated parameter.

The basic approach to sensitivity was taken from [Saltelli 2008]:

$$\overline{S}_i = \frac{f_{+\Delta k} - f}{\Delta p_k}, k = \{1,2,3, \dots, N_p\}, \quad (16)$$

where $\overline{S}_k$ is the sensitivity of k-th material parameter p_k and only k-th parameter is changed. We assume that $f > 0$, $k_{Sen} > 0$ and $p_k \neq 0$, then:

$$\begin{aligned} &\overline{S}_k = \frac{f_{+\Delta k} - f}{\Delta p_k} = \frac{f_{+\Delta k} - f}{p_k\, k_{Sen}} = \frac{1}{k_{Sen}}\left(\frac{f_{+\Delta k} - f}{p_k}\right) = \frac{1}{k_{Sen}}\left(\frac{f_{+\Delta k} - f}{f}\right)\frac{f}{p_k}, \\ &\overline{S}_k = \frac{1}{k_{Sen}}\left(\frac{f_{+\Delta k}}{f} - 1\right)\frac{f}{p_k} = S_k \frac{f}{p_k}, \\ &S_k = \frac{1}{k_{Sen}}\left(\frac{f_{+\Delta k}}{f} - 1\right), k = \{1,2,3, \dots, N_p\}. \end{aligned} \quad (17)$$

Where the sensitivity value S_k is a modified sensitivity. It was used in [Rojicek 2021]. The difference between $\overline{S}_k$ and S_k is demonstrated in Table 2. An effect of parameter change shows the column denoted as $|f_{+\Delta k} - f|$ and an absolute value is added to the sensitivity calculations. The values in Table 2 were calculated for the initial parameter values (see Table 1) and all experiments.

p_k		$k_{Sen} = 0.01$		
k	Parameter	$\lvert\overline{S}_k\rvert$	$\lvert S_k\rvert$	$\lvert f_{+\Delta k} - f\rvert$
1	E_{20} [MPa]	3.9 10^{-5}	0.26	0.00036
2	E_{80} [MPa]	1.7 10^{-5}	0.11	0.00031
3	μ [–]	0.17	0.22	0.00026
4	s_0 [MPa]	1.9 10^{-4}	0.014	3.6 10^{-5}
5	Q/R [K]	2.0 10^{-4}	6.34	0.0163
6	A [1/s]	2.1 10^{-5}	0.25	0.00073
7	x_i	0.11	2.2	0.0066
8	m [–]	1.9	1.78	0.0044
9	h_0 [MPa]	0	5.7 10^{-5}	2.0 10^{-7}
10	$\hat{S}$ [MPa]	2.1 10^{-2}	2.43	0.0059

11	**n** [–]	6.3	0.23	0.00029
12	**a** [–]	5.9 10^{-3}	0.034	9.0 10^{-5}

Table 2. Comparison of sensitivity estimates.

Values in the column $|f_{+\Delta k} - f|$ are dependent on the value of k_{Sen}, see parameter 1 for $k_{Sen} = 0.01$. The values in the column $|\bar{S}_k|$ differ significantly for parameters 2 and 11, although for a given value of k_{Sen} the values of the target function $|f_{+\Delta k} - f|$ changes almost the same. The value of $|S_k|$ better corresponds to the change in the value of objective function. Conversely, the value of $\bar{S}_k$ can be used in gradient algorithms. However, both values can be easily recalculated with respect to eqv (17).

By selecting the parameters with the highest and almost the same sensitivity values, their identification can be simplified. The simplification is due to the reduction of the number of parameters for identification. The second criterion, very similar sensitivity values for selected parameters, is based on the experience that parameters with very different sensitivity values are more difficult to identify (update algorithm, numerical noise, etc.). On the other hand, the number of cycles needed to identify the parameters increases and the calculation of the sensitivity values need to be repeated, because their values depend on the current value of the parameters. It can also be seen from Table 2 that parameter 9 has an order of magnitude lower effect on the result than the other parameters. This may be due to an inappropriate choice of parameters value or set of experiments. The given parameter should therefore be removed from the current identification process.

Some parameters can be identified separately, they are not searched for. In the paper, the Poisson number **μ** was taken from [Paska 2020], it was identified by Digital Image Correlation method.

For identification were select parameters with the haighese value of sensitivity $|S_k|$. For example, from Table 2, $k_{Sen} = 0.01$ we select parameters, 5, 7, 8 and 10 as follows:

$$\forall\, p_k \in X, \text{IF } 100\,|S_k| > 150 \text{ THEN } p_k \in \zeta, \quad \text{OTHERWISE } p_k \notin \zeta, \tag{18}$$

where ζ is a set of parameters for identification.

It is also possible to check whether the value of the parameter is not at the local minimum of the objective function:

$$f_{+\Delta k} > f < f_{-\Delta k}, k = \{1,2,3,\dots,N_p\}. \tag{19}$$

It is better to exclude from identification the parameter k that satisfies condition (19). But the total number of calculations for the selection of parameters increases to (2 Np + 1).

4.3 *Update method*

The Nelder-Mead Simplex method was used to determine the parameters, we used version given in [Lagarias 1998]. The method is appropriate for small dimensional problems [Han 2006]. The material model used has a total of $N_p = 12$ parameters, but the number of detected parameters can be reduced, as described in the previous chapter. Then, for the method the number of parameters for identification N_S was limited to $N_S \leq 4$. N_S also represents several dimensions for simplex, and $N_S + 1$ is a number of simplex vertices. We denote simplex vertices as $X_1, X_2, \dots X_{N_S+1}$, where the vertices are ordered according to the objective function values:

$$f(X_1) \leq f(X_2) \leq \cdots \leq f(X_{N_S+1}). \tag{20}$$

The algorithm uses operations : reflection, expansion, contraction and shrink. The algorithm used the centroid of the N_S best vertices:

$$\bar{X} = \frac{1}{N_S}\sum_{l=1}^{N_S} X_l. \tag{21}$$

A one iteration of the algrithm is defined by following steps :

Step 1. **Sort.** Evaluate $f(X_1), f(X_2), \dots, f(X_{N_S+1})$, and sort it.

Step 2. **Reflection.** $\alpha = 1$,

$X_r = \bar{X} + \alpha\,(\bar{X} - X_{N_S+1})$,

IF $f(X_1) \leq f(X_r) < f(X_{N_S})$ THEN $X_{N_S+1} \leftarrow X_r$, go to Step 1.

IF $f(X_r) < f(X_1)$ THEN go to Step 3

IF $f(X_{N_S}) \leq f(X_r) < f(X_{N_S+1})$ THEN go to Step 4.

IF $f(X_{N_S+1}) \leq f(X_r)$ THEN go to Step 5

Step 3. **Expansion** $\beta = 2$

$X_e = \bar{X} + \beta\,(X_r - \bar{X})$

IF $f(X_e) < f(X_r)$ THEN $X_{N_S+1} \leftarrow X_e$, go to Step 1.

ELSE $X_{N_S+1} \leftarrow X_r$, go to Step 1

Step 4. **Outside Contraction.** $\gamma = 0.5$

$X_{oc} = \bar{X} + \gamma\,(X_r - \bar{X})$

IF $f(X_{oc}) \leq f(X_r)$ THEN $X_{N_S+1} \leftarrow X_{oc}$, go to Step 1.

ELSE go to Step 6

Step 5. **Inside Contraction.**

$X_{ic} = \bar{X} - \gamma\,(X_r - \bar{X})$

IF $f(X_{ic}) \leq f(X_r)$ THEN $X_{N_S+1} \leftarrow X_{ic}$, go to Step 1.

ELSE go to Step 6

Step 6. **Shrink.** $\delta = 0.5$, For $2 \leq l \leq N_S + 1$

$X_l = X_1 + \delta\,(X_l - X_1)$, go to Step 1.

The effect of several initialization procedures is studied in [Wessing 2019]. We used some of the common initialization procedures. The first simplex vertex is given by the initial values of the parameters p_k, see Table 1. The others are updated from p_k by :

$$\begin{aligned} X_l = \{&\forall p_k \in \zeta: \\ &\text{IF } k = l \text{ THEN } p_k \leftarrow p_{-\Delta k} \\ &\text{OTHERWISE } p_k \leftarrow p_{+\Delta k} \\ &\forall p_k \in X/\zeta: \\ &p_k \leftarrow p_k\}, l = \{1,2,\dots,N_S\}. \end{aligned} \tag{22}$$

The update algorithm was stoped by the following condition :

$$f(X_{N_S+1}) - f(X_1) < 0.001\, f(X_1) \tag{23}$$

Before starting the FEM simulation, the constraints of the material parameters were checked as follows :

$$\begin{aligned} &\text{IF } p_k < p_{k,min} \text{ THEN } p_k = p_{k,min}, \\ &\text{IF } p_k > p_{k,max} \text{ THEN } p_k = p_{k,max}, \forall p_k \in \zeta. \end{aligned} \tag{24}$$

4.4 *FEMU algorithm*

In the paper is for determination of material parameters X used the FEMU algorithm, which is shown in Figure 2.

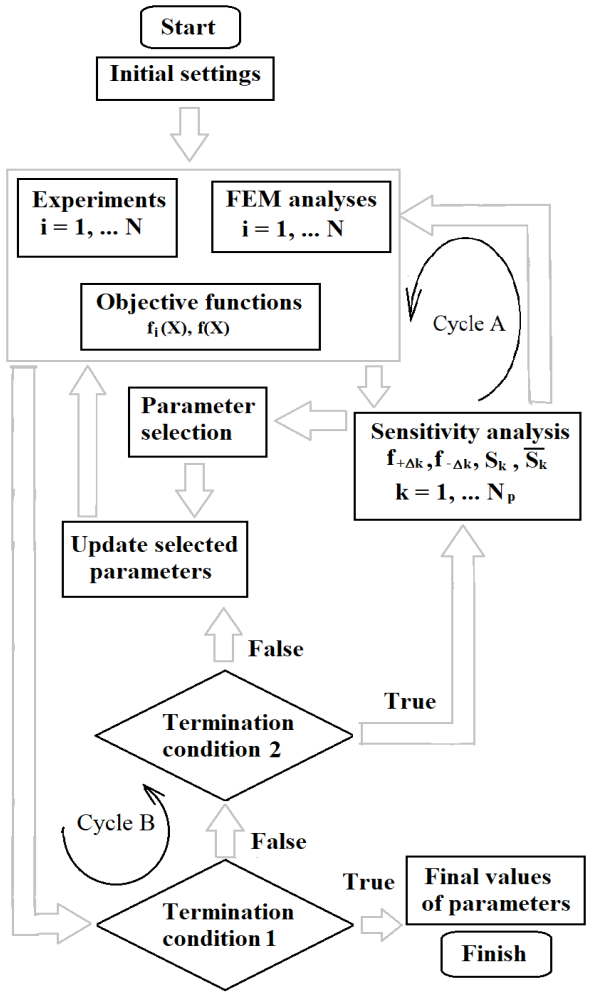

Figure 7. Schema of the FEMU algorithm

The algorithm includes the following steps:

Step 1. Simulation models of experiments are created, and initial values of parameters are specified.

Step 2. Simulations of all experiments are performed, the partial objective function and the objective function is calculated.

Step 3. Cycle A start, $f_{+\Delta k}$, $f_{-\Delta k}$, and f are calculated, S_k is calculated, Cycle A finish.

Step 4. Parameters for identification are selected (4 parameters).

Step 5. Cycle B start, the parameters are updated.

Step 2. Simulations of all experiments are performed, the partial objective function and the objective function is calculated.

Step 6. Termination condition 1 is applied. If the condition is met, Step 8 follows, otherwise Step 7.

Step 7. Termination condition 2 is applied, it is given by eqv (24). If the condition is met, Cycle B (Update algorithm) is finished, and Step 3 (Sensitivity analysis) follows. Otherwise, Step 5 follows, and Cycle B continues.

Step 8. Final values of parameters are determined.

The termination condition 1 has two parts, a convergence, and a sensitivity termination. The convergence criterion compares two values of the objective function - before the start of Cycle B and after the end of Cycle B. If the difference is small, less than $0.001\ f(X_1)$, the algorithm is finished. The sensitivity criterion is apparent from condition eqv (23), if it is satisfied for $\forall p_k \in X$, then the solution is terminated.

5 SIMULATION MODELS

FE model for simulation of indentation tests is shown in Figure 8. A/. The specimen for indentation was modeled as a block (10x10x7.5[mm]) with two symmetry planes. Because the fact that the simulation of indentation tests is significantly more time consuming than the simulation of tensile tests, a very coarse mesh was used. The specimen model was meshed with 1506, quadratic – 10-nodes, tetrahedral elements. The indenter was simulated as rigid. The bottom side of specimen's model was fixed, the rigid indenter's model was loaded. The loading states are given by the experiments and they are described in chapter 2.3.

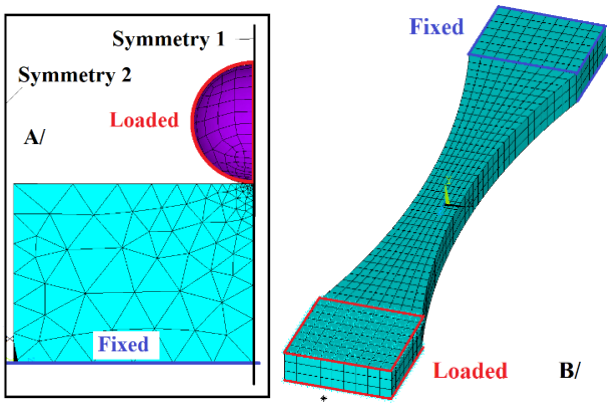

Figure 8. A/ FE model of specimen geometry with boundary conditions for simulation of indentation tests. B/ FE model of specimen geometry with boundary conditions for simulation of tension tests.

FE model for simulation of tension tests is shown in Figure 8. B/. The specimen dimensions are shown in Figure 1. The specimen model was meshed with 1880, quadratic – 20-nodes, hexahedral elements. The upper and lower nodes of the edge part of the sample's model were fixed and on the opposite side of the sample's model were loaded. The loading states are given by the experiments and they are described in chapter 2.1 and chapter 2.2.

6 IDENTIFICATON PROCESS

Identification of parameters is not the main goal of the paper, therefore the identification process is described only briefly and in general. The experiments will be denoted as follows:

1. Tension, 23 °C, 1.667 mm/s.
2. Indentation, 23 °C.
3. Tension, 44 °C, 0.017 mm/s.
4. Indentation, 44 °C.
5. Tension, 44 °C, 0. 167 mm/s.
6. Graded Tensile, 44 °C.
7. Tension, 60 °C, 0.017 mm/s.
8. Indentation, 60 °C.
9. Tension, 60 °C, 0. 167 mm/s.
10. Tension, 60 °C, 1.667 mm/s.
11. Graded Tensile, 60 °C.
12. Tension, 80 °C, 0.017 mm/s.
13. Indentation, 80 °C.
14. Graded Tensile, 80 °C.

The first identification is made from experiments 2, 4, 8 and 13. The constraints are shown in Table 3, These values were not found in the literature and are therefore estimated based on the authors' experience.

k	1	2	4	5	6	7
$p_{k,min}$	400	400	5	200	500	1
$p_{k,max}$	3000	3000	50	$2\ 10^4$	5000	20
k	**8**	**9**	**10**	**11**	**12**	
$p_{k,min}$	0.15	$5\ 10^4$	5	$1\ 10^{-5}$	0.5	
$p_{k,max}$	0.5	$5\ 10^5$	100	$1\ 10^{-2}$	5	

Table 3. Material parameters constraints.

The value of the objective function is calculated only from these experiments. The identification process is described by Table 4.

Cycle A	Cycle B	N_S	f(X)
Initial	-	-	0.2912
1	71	4	0.0633
2	61	3	0.0375
3	54	3	0.0327
4	7	3	0.0327

Table 4. Identification process - four indentation tests.

The second identification is made from experiments 1, 3, 5, 7, 9, 10 and, 12. The identification process is described by Table 5.

Cycle A	Cycle B	N_S	f(X)
Initial	-	-	0.235
1	120	3	0.04231
2	41	3	0.04077
3	10	2	0.04077

Table 5. Identification process - seven tension tests.

The last identification is made from all experiments 1-14. The identification process is described by Table 6.

Cycle A	Cycle B	N_S	f(X)
Initial	-	-	0.245
1	47	3	0.229
2	80	3	0.145
3	37	4	0.096
4	28	3	0.079
5	140	4	0.0541
6	68	3	0.0459
7	20	3	0.0457
8	51	3	0.0444

Table 6. Identification process from all tests.

7 RESULTS

Results are presented in figures and tables. Experimental data (EX) are displayed by solid lines, data from simulation models (FE) are displayed by dotted lines, $f_i(X)$ represents the partial objective function values, and i denoted the experiment, which was defined in previous section.

7.1 Identification from indentation tests

Values of material parameters determined form four indentation tests (2, 4, 8, 13) are shown in Table 7.

E_{20} [MPa]	E_{80} [MPa]	μ [–]	s_0 [MPa]	Q/R [K]	A [1/s]
2282	1212	0.33	19.5	9392	1648
x_i	m [–]	h_0 [MPa]	$\hat{S}$ [MPa]	n [–]	a [–]
4.74	0.2449	183245	30.9	0.0067	2.425

Table 7. Material parameters determined from four indentation tests.

Comparison of the indentation experiments with their FEM solutions is shown in Figure 9.

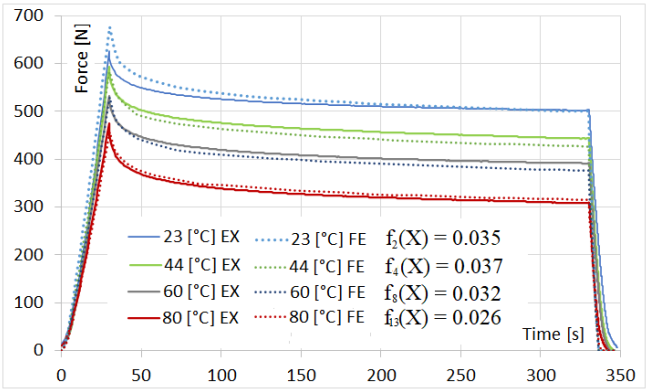

Figure 9. Comparison the data from indentation experiments (2,4,8,13) and from FE simulation with the values of their partial objective function.

The remaining experiments were used to validate the material parameters. The following Figure 10 shows tension experiments with the rate of deformation 0.017 mm/s and their FEM solutions.

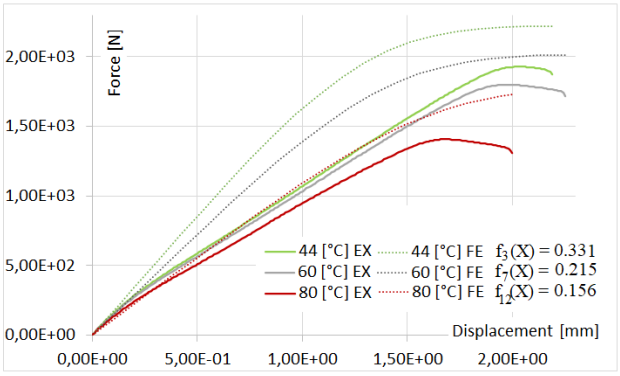

Figure 10. Validation of the parameters (Table 6), comparison the data from the tension tests 3,7,12 and from FE simulation (rate of deformation 0.017 mm/s) with the values of their partial objective function.

The values of the partial objective function from remaining experiments are described in Table 8.

$f_1(X)$ [–]	$f_5(X)$ [–]	$f_6(X)$ [–]	$f_9(X)$ [–]	$f_{10}(X)$ [–]	$f_{11}(X)$ [–]	$f_{14}(X)$ [–]
0.54	0.35	0.36	0.26	0.34	0.28	0.21

Table 8. The values of partial objective function for remaining validation experiments (1, 5, 6, 9, 10, 11, 14).

7.2 *Identification from tension tests*

Values of material parameters determined form seven tension tests (1,3,5,7,9,10,12) are shown in Table 9.

E_{20} [MPa]	E_{80} [MPa]	μ [–]	s_0 [MPa]	Q/R [K]	A [1/s]
1198	1093	0.33	19.5	9034	3134
x_i	m [–]	h_0 [MPa]	$\hat{S}$ [MPa]	n [–]	a [–]
6.846	0.3335	183245	31.0	0.0098	0.7863

Table 9. Material parameters determined from seven tension tests.

Comparison of the tension experiments with their FEM solutions is shown in Figure 11 – Figure 13.

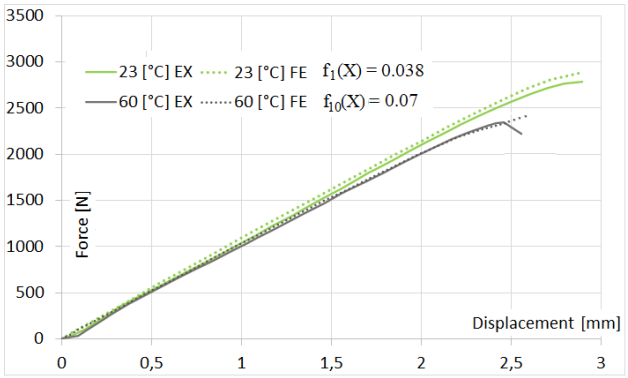

Figure 11. Comparison the data from tension experiments with the rate of deformation 1.667 mm/s (1, 10) and from FE simulation with the values of their partial objective function.

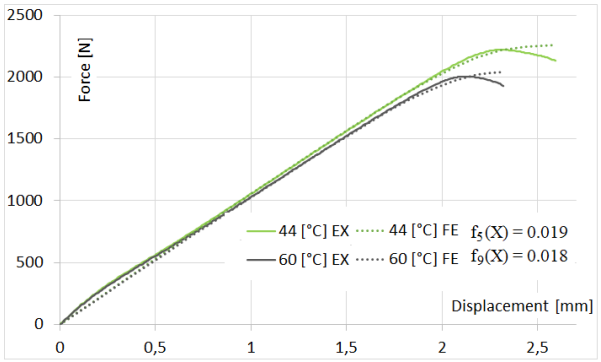

Figure 12. Comparison the data from tension experiments with the rate of deformation 0.167 mm/s (5, 9) and from FE simulation with the values of their partial objective function.

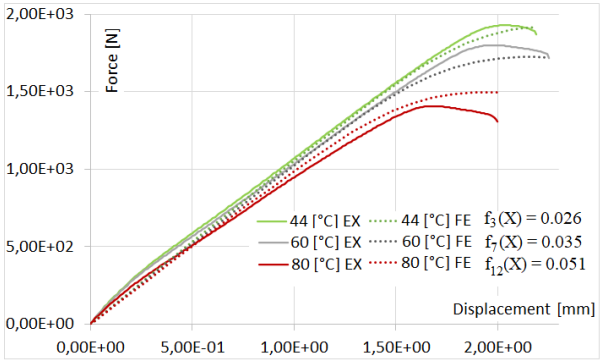

Figure 13. Comparison the data from tension experiments with the rate of deformation 0.017 mm/s (3, 7, 12) and from FE simulation with the values of their partial objective function.

The remaining experiments were used to validate the material parameters. The following Figure 14 shows the graded tension experiments (6, 11, 14) and Figure 15 shows the indentation experiments (2, 4, 8, 13).

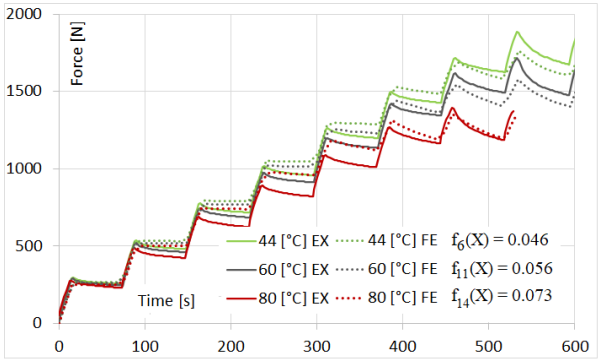

Figure 14. Validation of the parameters (Table 8), comparison the data from the graded tensile tests 6, 11, 14 and from FE simulation with the values of their partial objective function.

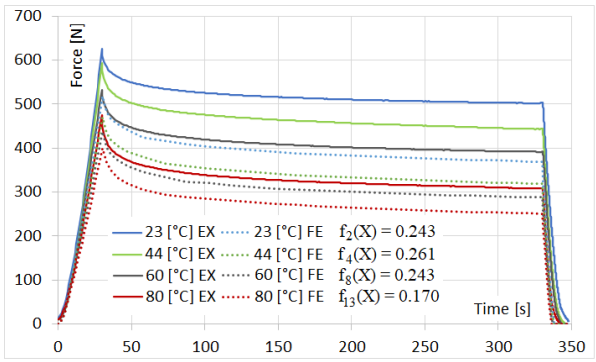

Figure 15. Validation of the parameters (Table 8), comparison the data from the indentation tests 2, 4, 8, 13 and from FE simulation with the values of their partial objective function.

7.3 *Identification from all tests*

Values of material parameters determined form all experiments (1-14) are shown in Table 10.

E_{20} [MPa]	E_{80} [MPa]	μ [–]	s_0 [MPa]	Q/R [K]	A [1/s]
1225	1093	0.33	19.5	8373	2612
x_i	m [–]	h_0 [MPa]	$\hat{S}$ [MPa]	n [–]	a [–]
11.1	0.373	183245	88.3	0.009782	3.38

Table 10. Material parameters determined from all experiments.

Comparison of selected experiments with their FEM solutions is shown in Figrue 16 – Figure 19.

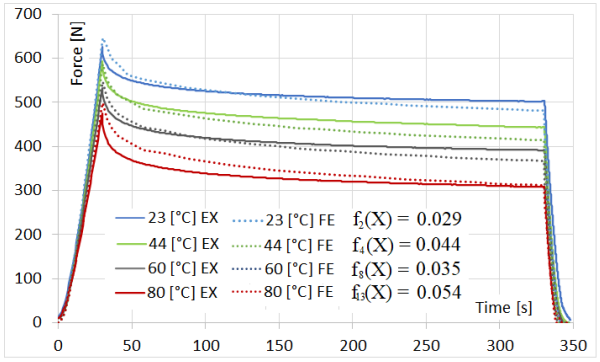

Figure 16. Comparison the data from indentation experiments (2,4,8,13) and from FE simulation with the values of their partial objective function.

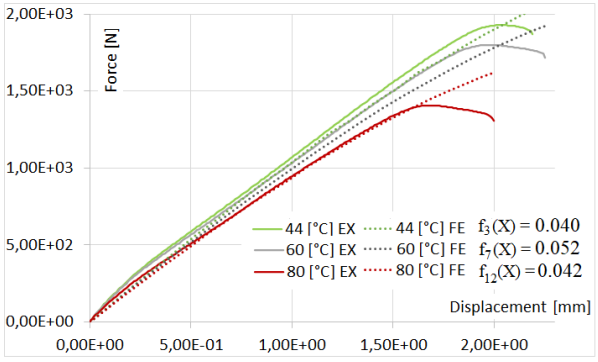

Figure 17. Comparison the data from tension experiments (3, 7, 12) and from FE simulation with the values of their partial objective function.

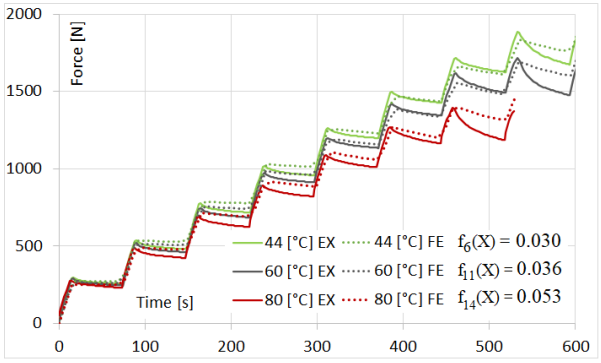

Figure 18. Comparison the data from graded tensile tests (6, 11, 14) and from FE simulation with the values of their partial objective function.

The values of the partial objective function from remaining experiments are described in Table 11.

$\mathbf{f_1(X)}$ [–]	$\mathbf{f_5(X)}$ [–]	$\mathbf{f_9(X)}$ [–]	$\mathbf{f_{10}(X)}$ [–]
0.044	0.033	0.035	0.073

Table 11. The values of partial objective function for remaining experiments (1, 5, 9, 10).

8 DISCUSSION

The value of the objective function for the initial estimation of the parameters was above 0.2, these values will be considered a bad result. The values of the objective function for the resulting parameters were below 0.055, on the contrary, we will consider these values as good results. With respect to eqv (11), the same values will be used to assess the partial objective functions.

The most interesting results are summarized in the following points:

- The resulting values of parameters obtained from the three identification processes are different (compare Table 7, Table 9, and Table 10). Some parameters are even twice as high (E_{20}, A, a).
- The parameters identified from indentation tests gives good results for these tests but wrong results for tensile tests and graded tensile tests.
- The parameters identified from tensile tests gives good results for these tests, acceptable results graded tensile tests and wrong results for indentation tests.
- The parameters identified from all tests gives good results for these tests, except for one (see Table 11, $\mathbf{f_{10}}$).
- It can be expected that with the increasing number of analysed experiments, the number of cycles needed to identify the parameters will also increase (see Table 4, Table 5 and Table 6).
- As the number of cycles increases, so does the value of the objective function for the best parameters (see Table 4, Table 5, and Table 6).

The following recommendations can be drawn from this:

IF the parameters are intended for simulations of various stress states, such as tension, pressure, multi-axis stress, contact, etc. **THEN** it is appropriate to include the required stress states in the identification or validation phase of these parameters.

By comparing the initial values of the parameters Table 1., and the resulting values of the parameters Table 7., Table 9. and Table 10., it can be seen, that some parameters do not change. This may be due to a very good initial estimate of the parameters, or the experiments used have too little effect on the parameters.

For a more detailed analysis of the above behaviour, we consider performing other experiments used in the identification process, such as pressure tests [Brown 1989], shear tests [Grama 2015], or combined torsion and tension tests [Rojicek 2010].

9 CONCLUSIONS

The influence of the selection of experiments on the identification results was analyzed. Two basic types of experiments were used, indentation tests and tensile tests. Three identification processes were performed: from indentation tests, from tensile tests and from all tests. The performed numerical experiments showed the influence of the selection of experiments on the result of the identification process, because the resulting parameters identified by the three independent processes are different. Validation performed on the remaining experiments confirmed the previous conclusion. On the other hand, the analysis was performed on only two types of experiments (tensile tests, indentation tests) and for one material model. Therefore, the next step will be to use a wider range of experiments to analyze the above behavior in more detail and to test other material models.

ACKNOWLEDGMENTS

This article was elaborated under support of the Research Center of Advanced Mechatronic Systems, reg. no. CZ.02.1.01/0.0/0.0/16_019/0000867, within the framework of the Operational Program for Research, Development, and Education.

REFERENCES

[Anand 1985] Anand, L., Constitutive Equations for Hot-Working of Metals. International Journal of Plasticity, International Journal of Plasticity. International Journal of Plasticity, 1985, Vol.1, No.3, pp 213-231, ISSN 0749-6419.

[Anrade 2007] Andrade-Campos, A., et al. On the determination of material parameters for internal variable thermoelastic–viscoplastic constitutive models. International journal of plasticity, August 2007, Vol.23, No.8, pp 1349-1379, ISSN 0749-6419.

[Brown 1989] Brown, S. B., et al. An internal variable constitutive model for hot working of metals. International journal of plasticity, 1989, Vol.5, No.2, pp 95-130, ISSN 0749-6419.

[Fusek 2021] Fusek, M., et al. Parameters Identification of the Anand Material Model for 3D Printed Structures. Simultaneous full-field multi-experiment

identification. Materials, February 2021, Vol.14, No.3, p 587, ISSN 1996-1944.

[Grama 2015] Grama, S., N., et al. On the identifiability of Anand visco-plastic model parameters using the Virtual Fields Method. Acta Materialia, March 2015, Vol.86, pp 118-136, ISSN 1359-6454.

[Han 2006] Han, L., Neumann, M. Effect of dimensionality on the Nelder–Mead simplex method. Optimization Methods and Software, 2006, Vol.21, No.1, pp 1-16, ISSN 1029-4937.

[He 2018] He, T., Liu, L., & Makeev, A. Uncertainty analysis in composite material properties characterization using digital image correlation and finite element model updating. Composite Structures, 2018, Vol.184, pp 337-351, ISSN 0263-8223.

[Inoue 2015] Inoue, N., et al. Andrade-Campos, A., et al. Prediction of viscoplastic properties of polymeric materials using sharp indentation. Computational Materials Science, December 2015, Vol.110, pp 321-330, ISSN 0927-0256.

[Lagarias 1998] Lagarias, J. C., et al. Convergence properties of the Nelder--Mead simplex method in low dimensions. SIAM Journal on optimization, Vol.9, No.1, pp 112-147, ISSN 1052-6234.

[Li 2013] Li, Xiao-qiang, and De-hua He. Identification of material parameters from punch stretch test. Transactions of Nonferrous Metals Society of China, 2013, Vol.23, No.5, pp 1435-1441, ISSN 1003-6326.

[Moslemi 2020] Moslemi, N., et al. Uniaxial and biaxial ratcheting behaviour of pressurized AISI 316L pipe under cyclic loading: Experiment and simulation. International Journal of Mechanical Sciences, 2020, Vol.179, ISSN 0020-7403.

[Neggers 2019] Neggers, J., et al. Simultaneous full-field multi-experiment identification. Mechanics of Materials, June 2019, Vol.133, pp 71-84, ISSN 0167-6636.

[Paska 2020] Paska, Z., et al. Methodology of arm design for mobile robot manipulator using topological optimization. MM Sci. J, June 2020, pp 3918-3925, ISSN 1805-0476.

[Rodgers 2005] Rodgers, B., et al. Experimental determination and finite element model validation of the Anand viscoplasticity model constants for SnAgCu. EuroSimE 2005. Proceedings of the 6th International Conference on Thermal, Mechanial and Multi-Physics Simulation and Experiments in Micro-Electronics and Micro-Systems, 2005, pp. 490-496.

[Rojicek 2010] Rojicek, J. Identification of material parameters by FEM. MM Sci. J, 2010, ISSN 1805-0476.

[Rojicek 2021] Rojicek, J. et al. Material model identification from set of experiments and validation by DIC. Mathematics and Computers in Simulation, Available online 24 April 2021, In Press, Corrected Proof, ISSN 0378-4754.

[Saltelli 2008] Saltelli, A., et al. Global sensitivity analysis: the primer, John Wiley & Sons, 2008, ISBN 978-0-470-72517-7.

[Touzeau 2016] Touzeau, C., Magnain, B., Emile, B., Laurent, H., & Florentin, E. Identification in transient dynamics using a geometry-based cost function in Finite Element Model Updating method. Finite Elements in Analysis and Design, 2016, Vol.122, pp 49-60, ISSN 0168-874X.

[Wessing 2019] Wessing, S., Proper initialization is crucial for the Nelder–Mead simplex search. Optimization Letters, Vol.13, No.4, pp 847-856, ISSN 1862-4480

[Yap 2019] Yap, Y. L., et al. A non-destructive experimental-cum-numerical methodology for the characterization of 3D-printed materials—polycarbonate-acrylonitrile butadiene styrene (PC-ABS). Mechanics of Materials, May 2019, Vol.132, pp 121-133, ISSN 0167-6636

CONTACTS:

Ing. Jaroslav Rojicek, Ph.D.
Department of Applied Mechanics
VSB – Technical University of Ostrava
Faculty of Mechanical Engineering
17. listopadu 15
708 33 Ostrava – Poruba
Czech Republic
e-mail Jaroslav.rojicek@vsb.cz
phone: +420 596 993 23